RSC Advances

PAPER

View Article Online
View Journal | View Issue

Cite this: *RSC Adv.*, 2025, **15**, 1275

Polyoxometalate-ionic liquids (POM-ILs) – a new type of ionic liquid additive family for lubricants†

M. L. Casasin-Garcia,[a] H. Khanmohammadi,[a] S. G. Mitchell[b] and N. Espallargas*[a]

Received 21st October 2024
Accepted 24th December 2024

DOI: 10.1039/d4ra07526a

rsc.li/rsc-advances

The focus on energy efficiency to move towards a more sustainable use of resources has intensified efforts to minimize friction and wear in mechanical systems, which account for 23% of the world's energy consumption. In this study, polyoxometalate ionic liquids (POM-ILs) are introduced as environmentally acceptable lubricant additives, for their potential friction-reducing and anti-wear (AW) properties. These compounds, characterized by their complex structures and tunable properties, have been investigated for their tribological performance across base fluids of varying polarities. Their performance has been compared against zinc dialkyldithiophosphate (ZDDP), a standard AW additive. Our findings demonstrate that POM-ILs exhibit promising friction-reducing and AW capabilities, comparable to traditional additives. The efficacy of POM-ILs was found to be highly dependent on the base fluid used, with significant variations observed in their ability to interact with stainless steel surfaces. Adsorption studies confirmed strong adsorption of POM-ILs onto stainless steel, with notable influence from the base fluid. Advanced characterization techniques revealed the formation of a predominantly oxide-rich tribofilm on the metal surface, as a result of POM-IL decomposition and reaction with the metal. POM-ILs show significant potential as lubricant additives, with their structural versatility offering a promising path for future greener developments in tribology.

1. Introduction

Renewable and greener sources of energy are nowadays a major focus in both research and industrial fields. However, greener energy sources still present an environmental impact, and the optimization of energy usage and minimization of energy loss is another powerful approach for more sustainable practices. One significant area for improvement in this regard is improving the energy inefficiency in mechanical systems. Indeed, 23% of the world's total energy consumption originates from mechanical systems through their tribological contacts, where 20% is used to overcome friction and 3% originates from wear and wear-related failures.[1–3] These energy losses are generally remediated by materials with a substantial environmental impact, such as zinc dialkyldithiophosphates (ZDDP), halogenated lubricant additives and mildly refined petroleum-based mineral oils,[4,5] amongst others. Material innovation without loss of practical performance is an essential step to work towards in the field of tribology. Thus, much industrial and academic effort is being made to upgrade today's lubrication technologies.

Lubrication, as the process, and lubricants, as the products, are used to reduce friction, but they also contribute to reducing heat, and wear between contacting surfaces in relative motion. Effective lubricants form a lubricating thin film that separates the contacting surfaces, providing a long-lasting and smooth operation life cycle. Lubricants are composed of base fluids, which are typically present in 70–99%, that are combined with functional additives in different quantities. Lubricant additives are tailored for a specific application, because different tribological systems have different oxidation, pressure, wear, and friction requirements, amongst others. Lubricant additives are especially crucial in the boundary lubrication regime, where the lack of a full lubricating film requires enhanced anti-wear (AW) action for reducing material and energy losses.

AW additives are a subclass of lubricant additives that activate at temperatures above 150 °C (depending on the type of chemical) during operation. This activation mechanism induces chemical reactions on the metal surface (tribochemical reactions), forming a protective layer, and thus reducing wear. Phosphorus containing additives are typical AW additives, where ZDDP is the most used. However, ZDDP has undesired environmental consequences since it produces toxic ashes in diesel internal combustion engines and is aquatoxic,[6] therefore, less harmful lubricant additives are to be identified and developed for minimizing environmental impact.

Since the early 2000s, the use of ionic liquids (ILs) in the field of tribology has grown exponentially; first as plain lubricants

[a]*Norwegian Tribology Center, Department of Mechanical and Industrial Engineering, Norwegian University of Science and Technology (NTNU), Trondheim, Norway. E-mail: nuria.espallargas@ntnu.no*

[b]*Instituto de Nanociencia y Materiales de Aragón (INMA-CSIC/UNIZAR), Consejo Superior de Investigaciones Científicas, Universidad de Zaragoza, Zaragoza, Spain*

† Electronic supplementary information (ESI) available. See DOI: https://doi.org/10.1039/d4ra07526a

and later shifting to additives.[7] ILs benefit from possessing tuneable chemical structures and properties such as negligible vapour pressure, high viscosity, thermo-oxidative stability and low melting point.[8] Crucially, their dipolar structure endows them with a high affinity for metallic surfaces, making adsorption and subsequent chemisorption possible.[9] Furthermore, their structures can be tailored to contain tribo-active elements such as P, B, N, S or F.[10,11]

The use of ILs as lubricant additives is relatively new and there are some uncertainties in terms of how they interact with metallic surfaces under tribological conditions. However, it has been reported that their improved lubrication and wear resistance is achieved through either physically adsorbed (physisorption) or chemically reacted (chemisorption) protective thin layers on the metallic surface as a consequence of thermal decomposition.[12] In both these potential scenarios, the anionic component is responsible for the direct interaction with the metal surface, and the cation follows as a secondary reagent or gets decomposed and degassed from the system as reported by Kawada *et al.*[13] The anion interacts preferably with the positively charged metallic surface after electrons are removed from it during the tribo-action or it is decomposed, and its components react with the nascent surface created during the mechanical action.[14] The anion is thus an important component of the IL and must be tailored according to the system needs. Elements that have shown good surface activity under tribological conditions for AW purposes include F, N, P, S, *etc.*, and are found in many traditional AW additives.[7] Their presence should be considered alongside alkyl chain length, functional groups, and electrostatic and stearic forces at play within the IL structures, so that solubility and stability in the base fluid is achieved, followed later by a good AW performance.

Conventional IL structures for tribological applications are generally based on a limited family of compounds. Zhou*et al.*[15] provide a summary of these structures, which are mostly based on ammonium, phosphonium, imidazolium, or pyridinium cations, and although the anionic moiety has more diversity (both organic and inorganic species have been reported), the majority are F-, P- and/or S-containing anions. Halogens present in the structures as well as some of the organic structures present in the cations can result in corrosion of the metal surfaces, are toxic and/or environmental hazards.[16,17] This has driven to the investigation of other structures, such as borates[18] amino acid-based ILs[19] and other bio-inspired IL structures.[20] This paper aims to contribute to this line of research by introducing a new family of IL materials based on inorganic anions (polyoxometalates) and bulky organic cations.

Polyoxometalates (POMs) are a wide family of anionic metal oxide clusters based on early-row transition metals in their highest oxidation state(s), *e.g.*, W, Mo, V, Ta and Nb; however, POMs of Fe, Cu, Pt, and Pd are also known. Solution-stable POMs are self-assembled in aqueous media through acidification of simple metal oxides. Their oxidation state, additional heteroatoms and arrangement leads to a large variety of cluster anions whose physicochemical properties can be tailored at the molecular level. POMs can be classified as iso- and heteropolyoxometalates, of general formulas $[M_mO_y]^{n-}$ and $[X_xM_mO_y]^{n-}$, respectively, where M = W, Mo, V, *etc.* and X = Si, P, As, *etc.* with $x < m$. POMs can also be classified as plenary or lacunary, where the former describes metal oxides with all cluster sites occupied, and the latter possessing vacant metal atom binding sites.

POMs have been studied since the 1800s, with the first, a phosphomolybdate, reported in 1826 by Swedish chemist, J. J. Berzelius.[21] Advancements in characterization techniques, such as X-ray crystallography, the 1900s facilitated a deeper understanding of these complex metal-oxide clusters. Emerging research on these molecules frequently centers on one of their inherent advantages, which is that they can be processed and adapted to a variety of purposes: they can be crystallised as alkali metal salts, hybridised with polymers, bound to nanoparticles, immobilized within porous framework, and combined with bulky organic cations (*e.g.*, alkyl ammonium and phosphonium cations) to produce polyoxometalate-ionic liquids (POM-ILs).[22–25]

POM-ILs have already been employed as functional materials in many fields, ranging from antibacterial and anticorrosion[23] to water purification,[26] and catalysis.[27] The hypothesis in this work is that the high negative charge, atomic composition, and chemical tunability makes POM-ILs relevant as potential lubricant additives. Since ILs have already shown significant promise in tribological applications, it can be reasoned that the deployment of POM-ILs further enhances the design opportunities arising from the potential to tune, at a molecular level, the inorganic and organic component parts to influence the electrostatic and steric forces as well as the interaction with metal surfaces. In addition, and as a part of a more efficient and environmentally improved performance, a multifunctional behaviour (both targeting, at least, wear and friction simultaneously) would be another desired outcome because it would reduce the amount of chemicals needed in the additive package of a lubricant. Reducing the amount of chemicals in a formulated lubricant can potentially suppress the antagonistic effects between additives, as well as reduce the demand for different chemical species overall. To test this hypothesis POM-ILs were incorporated into a variety of environmentally acceptable base fluids, including low viscosity polyalphaolefin (PAO8 with 8 cSt viscosity at 100 °C), dipropylene and diethylene glycol (DPG an DEG) and two synthetic esters: neopentyl glycol dioleate and 2-ethylhexyl palmitate. The polarity of the base fluids varies, with PAO8 being the least polar and esters the most polar, thus potentially exhibiting different compatibility with the POM-IL structures. Advanced surface characterization techniques were later used to evaluate the tribological properties of the POM-ILs on AISI 316L austenitic stainless steel.

2. Experimental

2.1. Materials

Table 1 and 2 show, respectively, the additives and base fluids used in this work alongside their structure and abbreviations. POMs and POM-ILs were synthesized in this work according to protocols published in the literature.[23,28]

Table 1 Chemical structure, molecular weight, and properties of the selected chemical additives

Additive	Mw (g mol^{-1})	Appearance	Abbreviation	Typical application
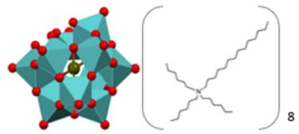 [Trihexyltetradecylammonium]$_8$[SiW$_{11}$O$_{39}$]	6409.4	Viscous, yellow liquid	SiW$_{11}$THTDA	Anti-corrosion and anti-bacterial coatings for natural stones[23]
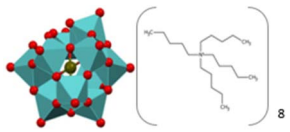 [Tetraheptylammonium]$_8$[SiW$_{11}$O$_{39}$]	5960.5	Hard gelatinous consistency, colorless	SiW$_{11}$THepA	Anti-corrosion and anti-bacterial coatings for natural stones[23]
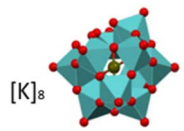 [K]$_8$ [SiW$_{11}$O$_{39}$]	2987.0	White powder	K$_8$SiW$_{11}$	Catalyst[29]
 Trihexyltetradecylammonium bromide	546.8	Viscous, yellow liquid	THTDABr	Cation used in lubricating and antibacterial ILs[23,30]
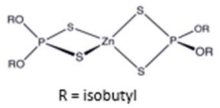 R = isobutyl Zinc dialkyldithiophosphate	547.8	Clear, viscous liquid	ZDDP	Traditional and effective antiwear additive[31]

Trihexyltetradecylammonium bromide (THTDABr) was purchased from Sigma Aldrich, and a primary ZDDP (Additin RC 3045) from TRiiSO LLC was used as a reference AW additive for comparison. The base fluids used for the lubricants included PAO8 (from Chevron Phillips); two glycols: DEG and DPG from Acros Organics; and two esters: neopentyl glycol dioleate (Dehylub 4016) and 2-ethylhexyl palmitate (Dehylub 4018) both from Emery Oleochemicals. All base fluids and additives were used as received with no further purification.

2.2. Preparation of lubricant formulations

10 mL of lubricant formulations were prepared with 1 wt% additives and 99 wt% base fluid, which is a standard composition in our research laboratory. The mixing process of the additives in the base fluids consisted of magnetic stirring for 6 hours at 60 °C followed by a 30 minutes ultrasonication (VWR USC300T model with a frequency and power of 35 kHz and 180 W respectively). Then, the lubricant formulations were visually assessed. Only the lubricants that appeared to have an adequate miscibility with the base fluid were selected for subsequent testing (discussed in further detail in Section 3.1).

2.3. Tribological testing

The tribological testing was performed with selected formulated lubricants on AISI 316L stainless steel substrate, which was obtained from a rod of 30 mm diameter that was cut into 6 mm thick discs. Prior to testing, the discs were prepared by grinding and polishing according to the guide provided by Struers,[33] to obtain an appropriate surface finish of Ra = 0.090 ± 0.003 μm. The cleaning after polishing consisted of ultrasonication in an ethanol–water bath (1 : 1) for five minutes, rinsing with water, and air drying. Then, a ball-on-disc tribometer (TriboCorr Resmat Corporation, Canada) was used to test the stainless steel discs under sliding reciprocal motion against a 6 mm diameter Al_2O_3 ball from Precision Ball and Gauge Co. Ltd, at 20 N normal load (corresponding to a maximum initial Hertzian contact pressure of 2.05 GPa). The sliding distance was 10 mm with a sliding frequency of 1 Hz, resulting in a linear velocity of 0.02 m s^{-1}. The duration of the test was 5000 cycles (20 mm per cycle), corresponding to a total sliding distance of 100 m. These tests were performed at room temperature. The calculated lambda value according to Hamrock–Dawson equation (which accounts for the ratio between the fluid film thickness and the

Table 2 Chemical structure and physicochemical properties of the base fluids tested

Base fluid	Mw (g mol^{-1})	Density (g cm^{-3})	Molecular formula	Abbreviation	Dipole moment (D)
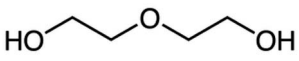 Diethylene glycol	106.1	1.118	$C_4H_{10}O_3$	DEG	1.26
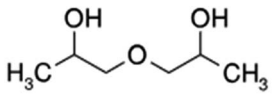 Dipropylene glycol (dimer mixture)	134.2	1.022	$C_6H_{14}O_3$	DPG	1.03
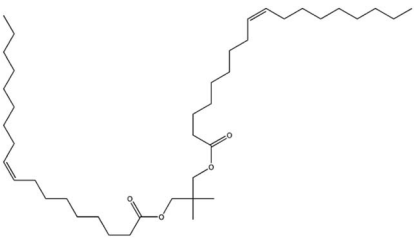 Neopentyl glycol dioleate (Dehylub 4016)	633.0	0.8982	$C_{41}H_{76}O_4$	DhL4016	5.85
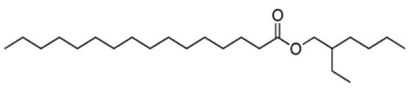 Ethylhexyl palmitate (Dehylub 4018)	368.646	0.8619	$C_{24}H_{48}O_2$	DhL4018	3.44
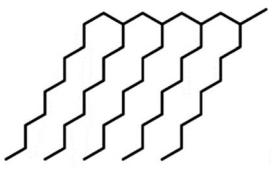 Polyalphaolefin 8 cSt	596[b]	0.833	N.A.[a]	PAO8	0.08

[a] The molecular structure for PAO8 is given as the generic polymerized PAO structure, since the composition of each specific PAO fluid is not generally disclosed given the polymerization variability. The hydrocarbon structure of PAO8 is not determined, since PAOs are the result of the oligomerization of linear α-olefins with a variable number of C in the alkyl chain. [b] Calculated values using a gas chromatography method.[32]

composite surface roughness of the moving pair)[34] resulted in values in the range of 10^{-2} for all the base fluids studied, corresponding to the boundary lubricating regime for all cases. All materials were tested at least twice to verify reproducibility of the results.

2.4. Adsorption studies

Adsorption of the additives to the metal surface was assessed with a Quartz Crystal Microbalance provided with dissipation monitoring (QCM-D) from Biolin Scientific. The sensors were stainless steel coated purchased from RenLux Crystal. The sensors were cleaned (by ultrasonication and UV-ozone cleaning) prior to each experiment. The experiment consisted of flowing through the tubing, at a constant flow of 50 μL per minute, the solution of the plain base fluid was then changed to the additive-containing solution, and lastly, the plain base fluid was run again. The frequency and the dissipation are measured against time during the whole process. The viscosity of the base

fluids (DPG and PAO8) only permitted the measurement of frequency and dissipation of the fundamental (1st) overtone.

Among the additives, only lubricants containing ZDDP and SiW_{11}THTDA were tested for consistency in both base fluids. SiW_{11}THTDA was diluted to 0.01 wt% due to instrumental limitations, while ZDDP was tested at concentrations of 1 wt% and 0.01 wt% to allow for a comprehensive analysis.

All tests were performed at least twice to verify reproducibility of the results.

2.5. Wear track characterization

The wear scar volume of stainless steel after tribological testing was measured using Alicona Infinite Focus optical 3D microscope (Bruker). Three wear volume loss measurements were taken for each wear track, at three different locations in the wear scar. The data was analyzed using MountainsMap software (Digital Surf). The wear volume was obtained by averaging the three measurements taken for each disc and the standard deviation was calculated. The averaged wear volume was used to calculate the specific wear rate (SWR) and the degree of material loss (β) according to the following equations:[35,36]

$$\mathrm{SWR} = \frac{\text{Wear volume}}{\text{Normal load} \times \text{sliding distance}} \quad (1)$$

$$\beta = \frac{A_{\text{groove}} - A_{\text{ridges}}}{A_{\text{groove}}} \times 100 \quad (2)$$

β approaches 0% when the material loss is only a consequence of plastic deformation, and it becomes 100% when the consequence for material loss is abrasive wear. Furthermore, a β-value of 100% means there is no material displaced to the sides of the wear track forming side ridges.

The wear track topography and primary surface assessment was studied by means of a Thermo Fischer Scientific (FEI) Quanta 650 field-emission gun (FEG) Scanning Electron Microscope (SEM), using an Everhart–Thornley detector (ETD). Additionally, with the help of Helios G5 plasma focused ion beam (PFIB), it was possible to prepare and observe the wear tracks cross sections. The preparation included the use of deposition, milling and polishing in the micrometer and nanometer scale, taking advantage of the plasma source. Carbon layers were deposited ahead of milling and polishing to protect the worn surface from the ion beam that could modify the surface composition. Once the deposition, milling and polishing was finished, cross section images were obtained through the secondary electron reaching the through-the-lens detector. Eventually, time-of-flight secondary ion mass spectrometry (ToF-SIMS) was performed, given the available detector on the same PFIB instrument.

For better resolution and chemical analysis, the process continued extracting a thin (less than 60 nm) lamella with the PFIB. Once achieved, the lamellae were studied with Scanning Transmission Electron Microscopy (STEM) using a retractable STEM detector on the same instrument. Finally, elemental mapping of this STEM lamellae was performed by an X-ray energy-dispersive spectrometry detector (EDS).

Surface chemical analysis X-ray photoelectron spectroscopy (XPS) was conducted on the wear track of the stainless steel disc tested with PAO8-SiW_{11}THTDA at different depths. The XPS analysis utilized a Kratos Axis Ultra instrument using a delay-line detector. The measurements were performed with a monochromatic Al Kα X-ray source, operating at a current of 10 mA and a voltage of 10 kV. During acquisition, the sample chamber pressure was maintained at 1×10^{-9} Torr. Depth profiling was achieved through ion milling with argon sputtering, using an argon energy of 4 keV and a pressure of 6.9×10^{-7} Torr. Seven data acquisition sets were obtained at varying etching times: 0, 5, 15, 35, 85, 185, and 685 seconds. Data analysis and curve fitting were subsequently performed using the CasaXPS software.

3. Results

3.1. Base fluid compatibility with additives

The solubility of all the chemicals listed in Section 2.1 was studied by blending the components and analysing the appearance of the lubricants. The solubility matrix presented in Table 3 shows three levels of solubility: non-soluble (×), fully soluble (✓) and partially soluble forming an emulsion-like liquid (E). In addition to the main base fluids (PAO, ester and glycol), water and a water–glycol 50 : 50 mixture (WG) were evaluated.

Due to the better compatibility of the POM-IL containing THTDA, its ionic liquid salt (THTDABr) was tested. THepABr was not tested due to the poor compatibility of its POM-IL with most of the base fluids.

The most polar base fluids, glycols and esters, showed overall better compatibility than the non-polar PAO8. Within the glycols, DPG solubilized both POM-ILs, becoming the most compatible base fluid. DhL4016 formed emulsions with the two POM-ILs becoming the most compatible of the two esters, which could be due to its higher polarity. Lastly, the most non-polar base fluid, PAO8, showed the least compatible behaviour, forming only one emulsion with one of the POM-ILs. Finally, water and WG mixtures only showed compatibility with the metal salt of the POM anion ($K_8SiW_{11}O_{39}$).

From Table 3, it is clear that the solubility of the POM-ILs in the base fluids can be a challenge. Polyoxometalates already present a multitude of possible assemblies and behaviors in solution[37] which accounts for the complexity of these species in aqueous media. Many of their challenges are mostly due to their pH and redox properties, which will be negligible in many base fluids in this study. In the absence of water, polarity, charge, and steric behavior can be more determinant factors for the solubility of POM and POM-related compounds in common base fluids.

DPG seemed to provide the best compatibility, with complete miscibility with both POM-ILs. The rest of the base fluids tended to form emulsions with these POM-ILs at room temperature. The resulting emulsions presented some different physicochemical properties, such as turbidity, which could be

Table 3 Additive solubility in base oil matrix

Additive solubility in base oils	DPG	DEG	DhL 4016	DhL 4018	PAO8	H_2O	WG
$SiW_{11}THepA$	✓	×	E	×	×	×	×
$SiW_{11}THTDA$	✓	×	E	E	E	×	×
THTDABr	✓	✓	✓	✓	×	×	×
$K_8SiW_{11}O_{39}$	×	×	×	×	×	✓	✓
ZDDP	✓	×	✓	✓	✓	×	×

the consequence of different saturation concentration for the different base fluids. Indeed, Dang *et al.*[38] claimed to improve the solubility of the POM-ILs in base fluids making them more non-polar by adding an organic coating. However, this approach was discarded for this work because the intention is to keep the structures as simple and functional as possible.

To account for the contribution of the individual components of $SiW_{11}THTDA$ on the compatibility with the base fluids, control experiments polar media included the potassium salt $K_8SiW_{11}O_{39}$ and the bromide salt THTDABr. The $K_8SiW_{11}O_{39}$ was soluble in water and in water–glycol media, but was found to be insoluble in glycols and esters; whereas THTDABr was only compatible with plain glycols and esters due to the presence of alkyl chains in its structure (Table 3). It is interesting the opposite compatibility behavior of $K_8SiW_{11}O_{39}$ and THTDABr, which probably accounts for the unpredictable solubility behavior of the POM-ILs in the different base fluids.

The emulsions formed by POM-ILs suggest that the presence of long alkyl chains significantly affects the compatibility between the POM-IL and the base fluid. $SiW_{11}THTDA$ forms emulsions both in PAO8 and the esters, whereas $SiW_{11}THepA$ only forms emulsions in PAO8. While PAO8 is non-polar, the esters have a localized dipole. Therefore, this polarity disparity seems less important for compatibility than the presence of long alkyl chains in the cation moiety. In contrast, DPG exhibits a different behavior, with both POM-ILs being fully soluble. The dimers of DPG have much shorter carbon chains and more oxygen per molecule compared to the esters and PAO8. Despite DPG's lower overall dipole moment, its dipole is more uniformly distributed, leading to different interaction with the POM-IL and thus resulting in better solubility.

Another possible explanation for the varying solubility of POM-ILs in these media could be a dynamic exchange of cation molecules with DPG molecules within the POM-IL cluster, which enhances the interaction between the base fluid and the solute (additive), resulting in better solubility. In contrast, the predominantly aliphatic nature of the esters and PAO8 likely creates a repulsion effect with the POM-IL cluster, favoring emulsion formation rather than a solution. In addition, the behaviour of DEG, which is structurally similar to DPG, differing only in one carbon atom, indicates that the dimeric structure of DPG plays a crucial role in its compatibility with POM-ILs.

Furthermore, the shorter alkyl chains in THepA seem to hinder its compatibility with the esters and PAO8 but not with DPG. This observation further suggests that POM-IL-DPG compatibility is primarily mediated by electrostatic interactions. On the other hand, POM-ILs compatibility with esters and PAO8 suggests that the governing phenomenon are steric hindrance and repulsions of aliphatic chains. Consequently, a longer alkyl chain in the cationic moiety will enhance compatibility of POM-ILs in non-polar base fluids such as PAOs and in aliphatic, such as esters.

ZDDP was soluble in the two esters, PAO8 and DPG, but not in DEG, water and water–glycol, following a similar compatibility to $SiW_{11}THTDA$, except that ZDDP was fully soluble in PAO8 and the esters.

3.2. Friction results

The friction results consisted of coefficient of friction (COF) *vs.* distance (m) plots, which are all available in the ESI.† The average COF values (including the running in period) are summarized in Table 4.

All friction tests, except for DPG repetition 1 exhibited a running in period, being longer in the case of PAO8. Moreover, none of the additives tested in DPG improved friction compared with the plain base fluid, and some even increased the average COF. On the other hand, both additives in DEG decreased friction, but the COFs in DEG lubricants were higher than in DPG.

In the case of the esters (DhL4016 and DhL4018) the running-in period was rather short with a sharp drop. Not all POM-ILs were compatible with DhL4018, but $SiW_{11}THTDA$ was compatible in both esters leading to lower friction in DhL4018. Overall, DhL4018 resulted in lower COF, both with and without additives.

Finally, all PAO8 based lubricants showed a running in period, and an average COF close to 0.5 in the case of plain PAO8. ZDDP showed a considerably shorter running in period with the lowest friction. Both $SiW_{11}THTDA$ and ZDDP additives reduced the average friction after the running in.

3.3. Wear rate

Fig. 1 and Table 4 show the SWR and β values measured, respectively, for all samples after tribological testing.

The wear rate for DPG was only decreased by ZDDP and THTDABr. The other glycol tested in this work (DEG) had the largest wear rates of all tests, and none of the POM-ILs could be evaluated for SWR.

As for the esters, DhL4016 resulted in the highest wear rate, twice as much as DhL4018. All additives seemed to have some

Table 4 Averaged COF and β value for each tribotest

	Repetition 1				Repetition 2			
Blend	Avg. COF running in	Duration running in (m)	Avg. COF	β (%)	Avg. COF running in	Duration running in (m)	Avg. COF	β (%)
Plain DPG	—	—	0.1719	99.89	0.1828	1	0.1715	99.65
SiW11THTDA in DPG	—	—	0.1802	99.64	—	—	0.1714	99.61
SiW11ThepA in DPG	—	—	0.1809	99.79	—	—	—	—
THTDABr in DPG	—	—	0.1748	99.64	0.1875	1	0.1765	99.71
ZDDP in DPG	—	—	0.1909	99.70	0.1839	1	0.1626	99.24
Plain DEG	0.3325	1	0.2508	88.81	0.3164	1	0.2504	93.82
THTDABr in DEG	0.2933	1	0.2252	94.78	0.2843	1	0.2129	97.44
Plain DhL4016	0.1448	2	0.1453	99.54	0.1574	2	0.1462	99.79
SiW11THTDA in DhL4016	0.1577	2	0.1529	99.85	0.1576	2	0.1415	99.75
SiW11ThepA in DhL4016	0.1413	2	0.1426	99.86	0.1559	2	0.1415	99.61
THTDABr in DhL4016	0.1727	2	0.1426	99.78	0.1561	2	0.1486	99.92
ZDDP in DhL4016	0.1533	2	0.1435	99.62	0.1573	2	0.1431	99.73
Plain DhL4018	0.1447	2	0.1338	99.73	0.1326	3	0.1224	99.11
SiW11THTDA in DhL4018	0.1372	2	0.1241	99.63	0.1380	3	0.1260	99.51
THTDABr in DhL4018	0.1452	2	0.1222	99.46	0.1293	1	0.1134	97.93
ZDDP in DhL4018	0.1326	2	0.1227	99.42	0.1329	1	0.1213	95.38
Plain PAO8	0.5052	45	0.2242	86	0.4258	35	0.1657	66.14
SiW11THTDA in PAO8	0.3197	11	0.1194	47.71	0.3052	15	0.1214	34.95
ZDDP in PAO8	0.2041	5.5	0.1165	58.67	0.1802	5	0.1219	42.98

reducing wear ability in DhL4016, however, ZDDP had the most wear reducing ability. All additives significantly reduced wear in DhL4018, with ZDDP being the most efficient.

The lowest wear of all tested additives was observed in PAO8. However, wear reduction was most significant for the POM-IL and ZDDP, both having a similar impact on wear rate reduction.

Table 4 shows very high β values for all glycol and ester-based lubricants, evidencing mostly abrasive wear. Contrary, PAO8 lubricants showed more variable values, revealing contributions from both abrasive wear and plastic deformation. Interestingly, SiW_{11}THTDA and ZDDP in PAO8 showed the lowest β values of all tests, evidencing the highest degree of plastic deformation within the test matrix.

After the compatibility study, and the friction and SWR screening, SiW_{11}THTDA and ZDDP were selected for more detailed analysis due to their clearly best performance in the base fluids.

3.4. Wear track characterization

The morphologies of the wear tracks of the selected formulated lubricants were studied using SEM (Fig. 2). By comparing SiW_{11}THTDA and ZDDP wear track morphologies with the one obtained in the plain base fluids, it was possible to evaluate the effect of the interaction between the base fluid and these additives. Additional SEM images can be found in Table S1 in the ESI.†

As anticipated by the β values, the glycol and the esters showed signs of surface abrasion, ZDDP-DPG showed some cracks and irregularities as well as abrasion marks, and SiW_{11}THTDA showed evidence of abrasion to a similar extent to plain DPG.

For the esters, both plain DhL4016 and DhL4018 showed a low level of wear damage, however ZDDP appeared to decrease the abrasion marks. SiW_{11}THTDA reduced abrasion in the case of DhL4016 but showed increased surface cracking for DhL4018. Therefore, because of these results and their poorer compatibility with SiW_{11}THTDA compared to DPG (Table 3), the esters will not be further studied in more detail.

Compared to plain PAO8, a significant reduction in wear damage is observed with both ZDDP-PAO8 and SiW11THTDA-PAO8. This could likely be attributed to the formation of a protective tribofilm on both surfaces. Whether this tribofilm formation was mediated by adsorption or chemical interaction with the surface is discussed in the upcoming sections.

3.5. Tribofilm characterization

A more in-depth analysis with FIB and S(T)EM-EDS of the best performing samples (SiW_{11}THTDA and ZDDP in both PAO8 and DPG) was performed to study the wear and frictional performance of these lubricant formulations. The FIB cross-sectional images, along with the corresponding S(T)EM and oxygen EDS map are shown in Fig. 3 and 4.

In Fig. 3, the FIB image corresponding to the wear track cross section of SiW_{11}THTDA in PAO8 showed a very large (around 3.5 μm thick) plastically deformed area (this area is denoted with a dashed-green line in the image), which is confirmed by the S(T)EM images. At the very top of the S(T)EM image, a lighter layer evidencing the presence of an oxide rich tribofilm was found and confirmed by EDS mapping. ZDDP in PAO8 showed a much thinner refined grain structure (around 500 nm thick) with hints of some patched surface layer on the wear track which could be observed in a darker color at the interface with the protective carbon layer in the FIB-SEM image. The S(T)EM image of ZDDP in PAO8 highlighted this tribofilm, which is rich in oxygen on the EDS mapping. The remaining EDS elemental mapping can be found in Fig. S7 in the ESI,† where the presence

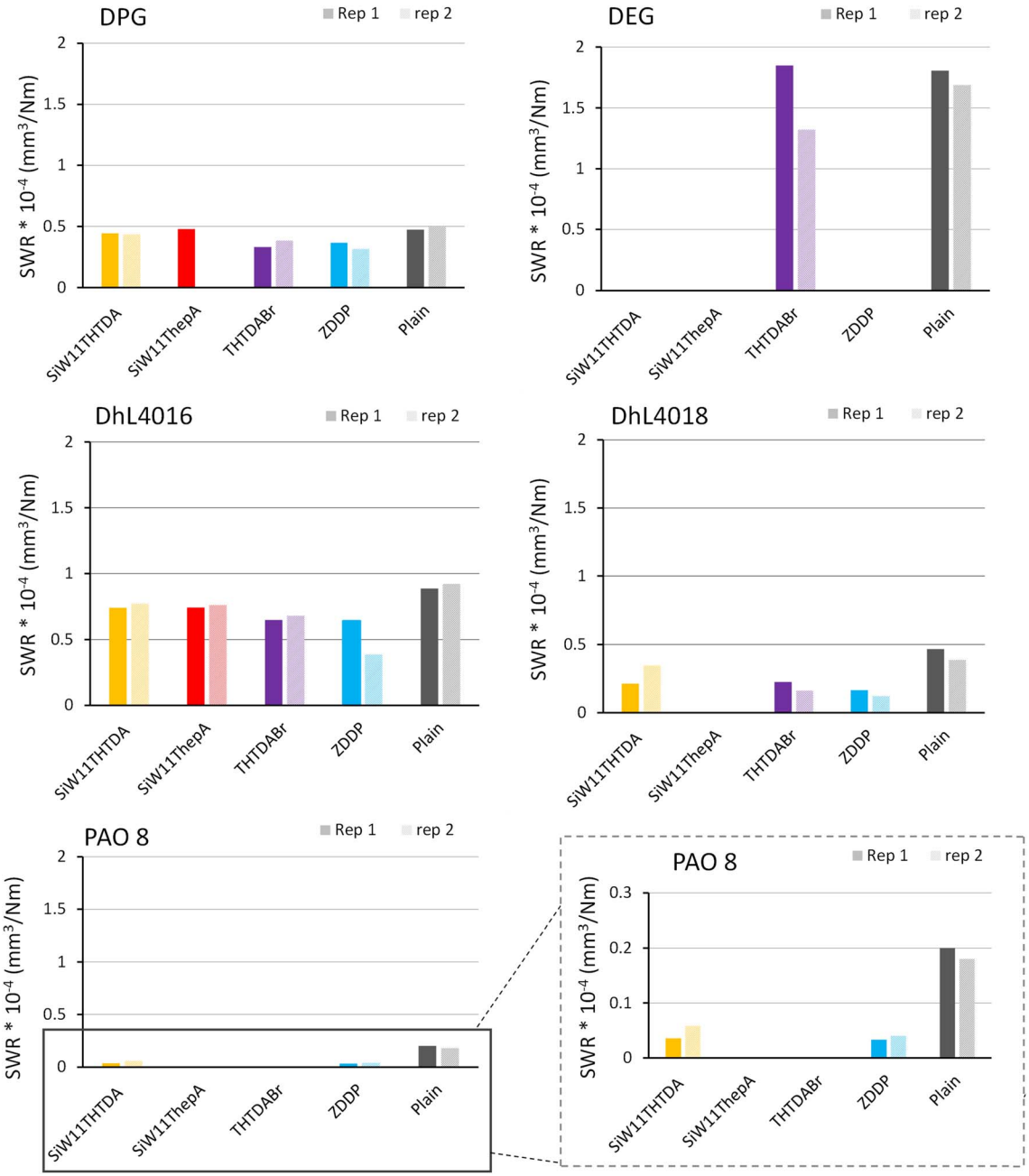

Fig. 1 Specific wear rate ($mm^3\ Nm^{-1}$) of both repetitions of the tested samples.

of S, Fe, P, O and Zn were found to a smaller extent. This is in agreement with previous literature that described the ZDDP tribofilm to consist of a mixture of Zn/Fe polyphosphates and precipitates of Zn/Fe sulphides.[39] This patch-like tribofilm covers the surface less effectively than the layer formed by SiW_{11}THTDA.

On the other hand, SiW_{11}THTDA in DPG (Fig. 4) showed a less plastically deformed subsurface layer and there was no visual evidence of any tribofilm. Similarly, ZDDP in DPG showed a smaller deformation area than in PAO8 and no evidence of tribofilm formation. Overall, both additives in DPG displayed a similar surface modification pattern. The EDS mapping of SiW_{11}THTDA and ZDDP in DPG showed the absence of a tribofilm, even if the presence of oxides was deeper within the subsurface structure, this was probably a consequence of smearing of wear debris under frictional forces and stress.

3.6. Adsorption results

The QCM-D measurements were carried out to study the adsorption behaviour of SiW_{11}THTDA and ZDDP in PAO8 and DPG. Fig. 5 shows the frequency (Δf) and dissipation (ΔD) changes with time obtained from the QCMD tests. In the case of PAO8 a frequency drop takes place when the base fluid containing additives is pumped in the cell, whereas the opposite

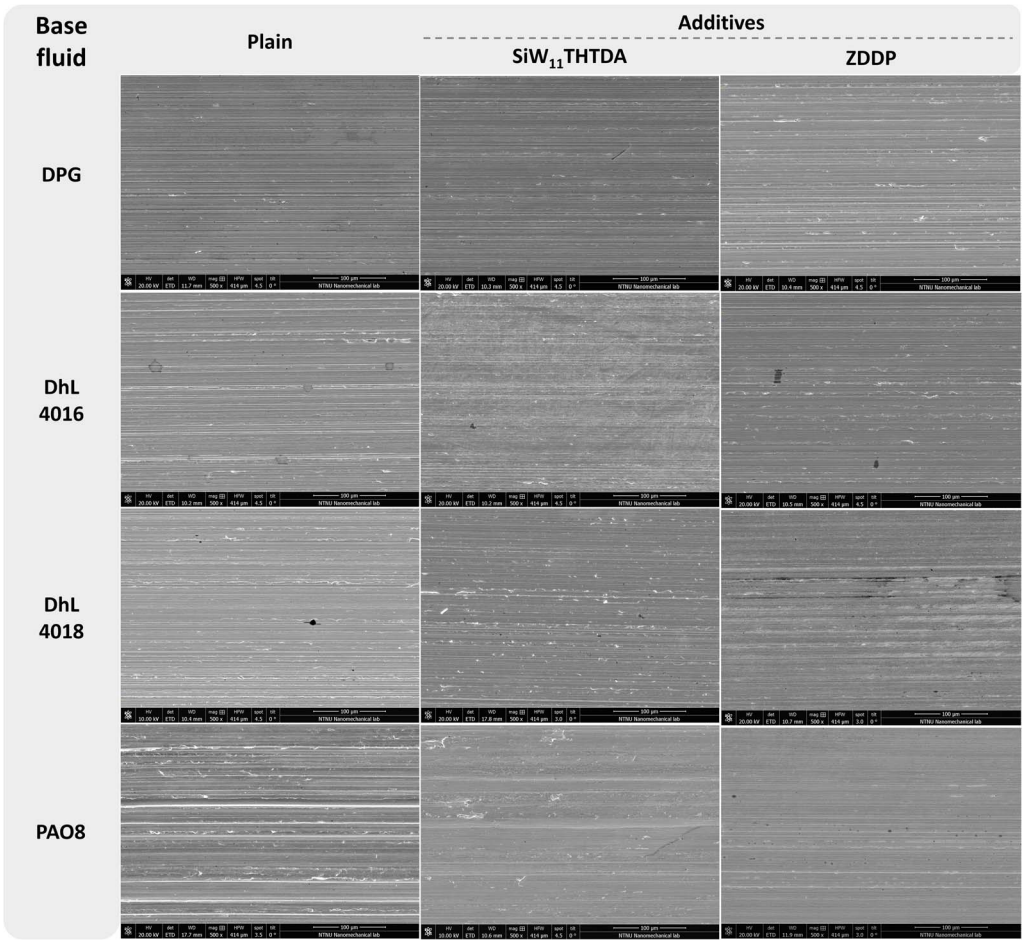

Fig. 2 SEM images (500× magnification) of the wear tracks on stainless steel after testing of selected formulated lubricants.

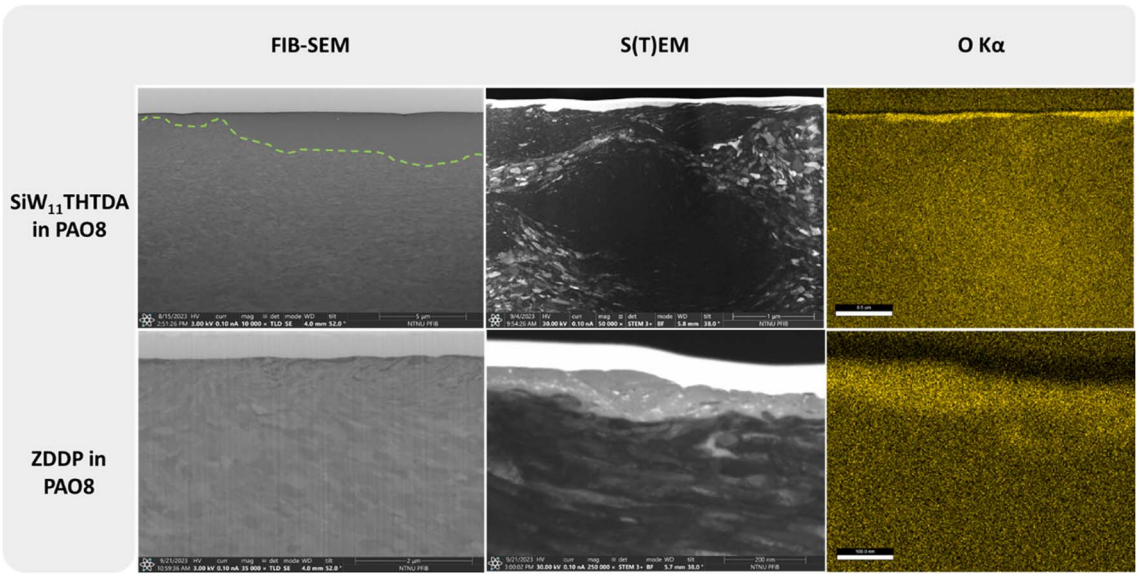

Fig. 3 Cross section images and elemental mapping of the wear tracks of $SiW_{11}THTDA$ and ZDDP in PAO8.

was found for DPG. In the case of $SiW_{11}THTDA$, a test at 1 wt% concentration was carried out, for consistency with the rest of the experiments. However, the very large frequency drop, of around 6000 Hz, created problems with the acquisition of a complete experiment, and therefore, a concentration reduction of this additive to 0.01 wt% was necessary for obtaining the

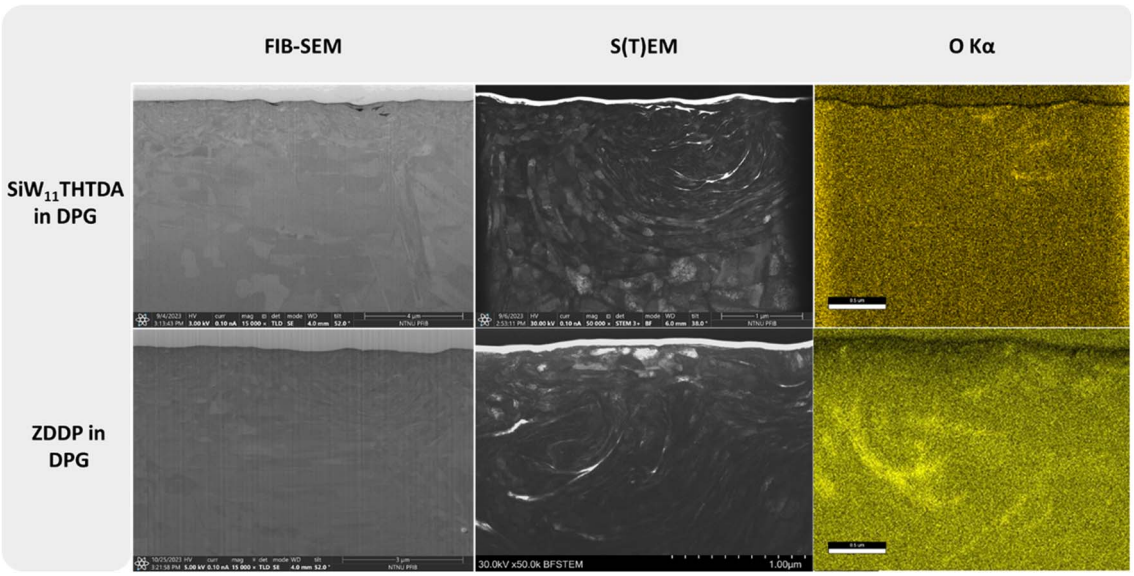

Fig. 4 Cross section images and elemental mapping of the wear tracks of SiW_{11}THTDA and ZDDP in DPG.

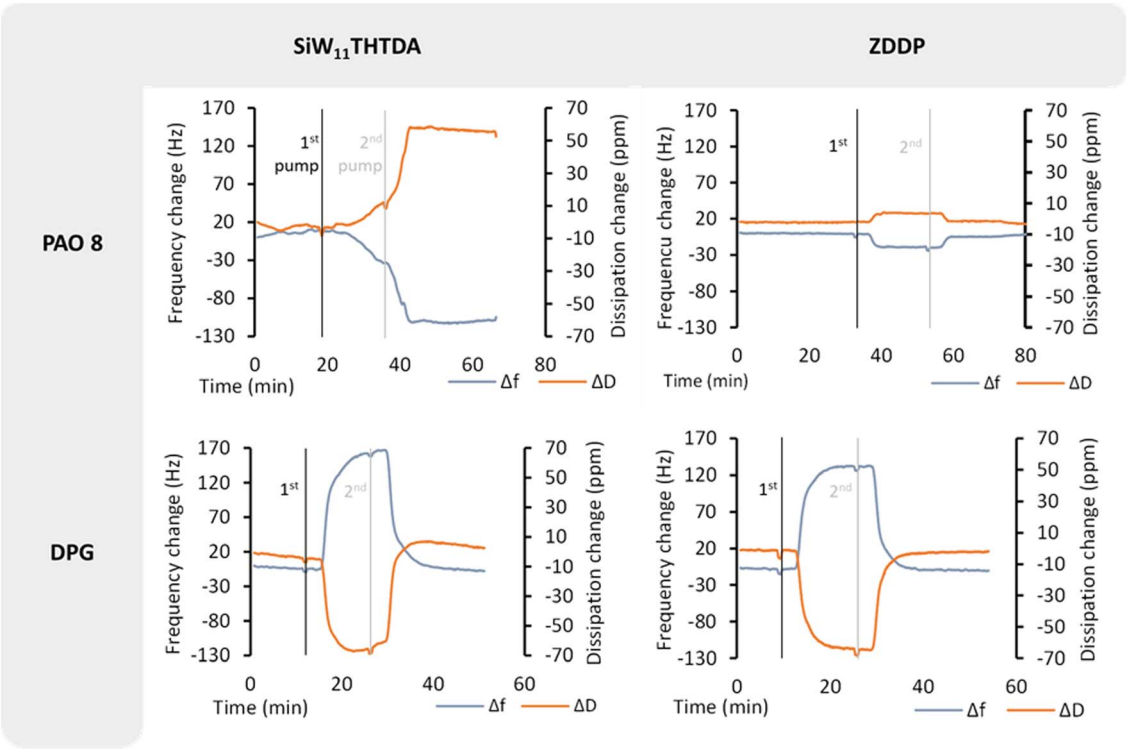

Fig. 5 QCM-D plots *versus* time, showing frequency change and dissipation for the four tested lubricants. Vertical lines represent pumping changes. The 1st darker line accounts for the addition of the additive, and the 2nd line corresponds to the pumping of base fluid for flushing or rinsing.

experimental data. During the test at 0.01 wt% concentration, the frequency drop stayed at low levels after flushing with the plain base fluid, indicating a strong adsorption, or chemisorption, onto the sensor. On the other hand, the frequency drop of ZDDP in the same base fluid increased again after flushing with the plain base fluid as indicative of a physisorption process.

Very different behaviour was observed in the case of DPG where the frequency change was positive (frequency increased as the additive got introduced). This change in frequency, however, went back to the initial point after flushing with the plain base fluid, indicating again a weakly adsorbed film of both additives onto the sensor.

4. Discussion

4.1. Effect of base fluid on additives' adsorption

Sauerbrey in 1959 proposed the following relationship between the resonant frequency and mass change upon the addition of a foreign layer onto a quartz crystal sensor:[40]

$$\Delta f = -\frac{2{f_0}^2}{A\rho_q}\Delta m \quad (3)$$

where Δf and Δm represent changes in resonant frequency and in mass, respectively, f_0 is the fundamental frequency of the quartz crystal under vacuum, A is the available area of the crystal and ρ_q accounts for the quartz density. This equation disregards the viscoelastic effects of the adsorbed layer, which can significantly affect the frequency. In this work, a QCM with dissipation mode was used so, the energy loss or dissipation (ΔD) was measured as well. Dissipation measures properties related to the viscoelastic properties of the adsorbed layer.

One of the proposed mechanisms of the working principles of ILs as lubricant additives describes how ILs have a high affinity towards metallic surfaces, where first the anion, and later the cation adsorb onto it, followed by other ILs, possibly creating a multilayer structure.[41,42] This cannot be confirmed for POM-ILs in this work since one would need to measure more than the fundamental overtone in QCM, but the strong chemisorption process observed in Fig. 5 implies a strong interaction with the metal surface, which is evident for POM-ILs in PAO8.

As mentioned in Section 3.6, the adsorption experiment for SiW_{11}THTDA had to be performed at a much-diluted concentration (100 times) because of the large frequency drop. When the same experiment (0.01 wt% concentration) was performed for ZDDP in PAO8, no frequency drop was observed (Fig. 6). At 1 wt% ZDDP concentration (Fig. 5) however, a frequency drop upon addition of the additive was observed. This frequency drop reversed upon flushing with the plain base fluid, indicating weaker adsorption compared to the POM-IL. Furthermore, in Fig. 5, the frequency drop for 1 wt% ZDDP was much smaller than that for the 0.01 wt% POM-IL, despite the POM-IL being 100 times more diluted. This illustrates the significantly higher change in adsorbed mass for the POM-IL. Given that the molecular mass of ZDDP is almost 12 times lower than SiW_{11}-THTDA (Table 1), the adsorption of a ZDDP molecule yields a much smaller mass on the sensor than SiW_{11}THTDA for the same number of adsorbed molecules. However, the observed frequency drops suggest a much greater mass change than what would be expected for the difference in molecular mass only, indicating a much more efficient surface adsorption of SiW_{11}-THTDA compared to ZDDP. These differences in adsorption can be directly linked with the frictional behaviour, since a stronger adsorbed layer will lead to lower interfacial shear. Indeed, this seems to be the case as illustrated in Fig. 4 although it is not as pronounced as indicated by the adsorption measurements. Under tribological testing, the sliding motion constantly removes the adsorbed layer, and the mechanical contact creates high local temperature and pressure. Under QCM-D, the testing conditions are static, and the test is performed at room temperature. Therefore, the observed differences in friction between the POM-IL and ZDDP are not solely result of adsorption but might have been also affected by tribochemical processes triggered by high local temperature and pressure that cannot be replicated by QCM.

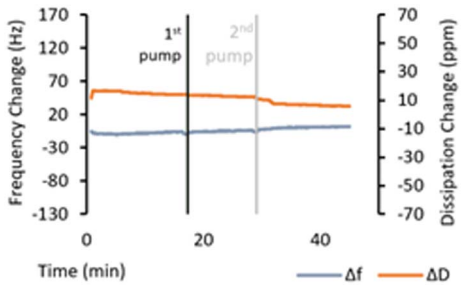

Fig. 6 QCM-D plots *versus* time, showing frequency change and dissipation for ZDDP at 0.01 wt% in PAO8.

For DPG, both the POM-IL and ZDDP exhibited similar behaviour. The observed frequency rise was associated to the layer viscoelastic contribution rather than the adsorption mass contribution, as reported by an independent study conducted by Wijanarko *et al.*[14] The positive frequency shift and the negative dissipation shift implies thus that the adsorbed layer had both low shear viscosity and a low shear elasticity modulus compared to the bulk liquid. This can be an indicative of surface adsorption competition and can therefore justify the higher friction observed for ZDDP and SiW_{11}THTDA in DPG compared to PAO8.

Overall, the observed friction, wear, and adsorption results indicate that DPG did not provide an adequate environment for the tested additives in stainless steel substrates. In contrast, PAO8 demonstrated better performance as a base fluid for the additives, most likely due to the absence of competition for the adsorption surface sites.

4.2. Additives' thermal decomposition effects on tribofilm formation

Both additives in PAO8 can efficiently reach the surface since the base fluid does not have a high affinity for the metal surface. However, adsorption analysis alone did not fully explain the friction and wear results. High resolution microscopic analysis of the wear tracks provided additional insight into friction and wear mechanisms. The cross-section images of the wear tracks in Fig. 3 and 4 show strong interaction between the metal surface and the additives, as well as the subsequent physicochemical changes on the surface. SiW_{11}THTDA appeared to readily interact with the metallic surface in PAO8. Therefore, the tribofilm observed in the STEM-EDS mapping likely resulted from a tribochemical reaction aided by the chemisorption of the POM-IL. Under the high contact pressure and temperature during the tribotest, the POM-IL likely decomposed and reacted with the surface, forming a protective layer against further wear. Thermogravimetric analysis (TGA) of SiW_{11}THTDA (Fig. S8†) revealed that 42% of the mixture decomposes at temperatures below or equal to 600 °C, which are locally reachable during

a tribotest. Mass calculations indicate that this weight loss mainly corresponds to the cation decomposition, a finding consistent with the literature.[43] This decomposition likely facilitates tribofilm formation by increasing exposure of the POM moiety to the stainless steel surface.

Interestingly, surface chemical analysis by ToF-SIMS and XPS (Fig. 7 and 8) showed that both tungsten and tungsten oxide are present in different oxidation states along the wear track for the tests performed with SiW_{11}THTDA in PAO8. This result further supports the hypothesis that SiW_{11}THTDA decomposed into its constituent elements, which then reacted with the elements of the stainless steel to form a protective tribofilm.

The different oxidation states of tungsten on the wear track found with ToF-SIMS were: W(I), W(III) and W(V).[44,45] Given that the tungsten in SiW_{11}THTDA is initially in the +6 oxidation state, the presence of +1, +3 and +5 oxidation states suggests that electron gain processes reduced the original W(VI). However, it is difficult to determine if these redox processes were solely a consequence of the tribochemical processes or if the ion beam used in the ToF-SIMS influenced the redox reaction. To better understand this reduction process, XPS analysis was also performed.

Fig. 8 shows the tungsten peak and illustrates the evolution of the oxidation states as etching progresses deeper into the metal surface. Comparing the W-based compounds present on the shallower surface in Fig. 8a (5 seconds etching, under 1 nm depth) and the deeper surface in Fig. 8b (685 seconds etching, approximately 23 nm depth) clear differences were observed.[46] At the outer surface, tungsten was mostly found as WO_3 with oxidation state VI (~99 at%), the same as the original POM-IL. As etching progressed, the signal of other oxidation states increased. At around 23 nm depth, the distribution of W compounds was as follows: metallic W(0) (at ~18 at%), WC(IV) (at ~11 at%), and WO_2 (IV) (at ~5 at%), with the remaining corresponding to WO_3 (VI) (at ~67 at%). Despite the depth, most of the tungsten remained in oxidation state VI, though significant changes occurred deeper into the surface. This could support the hypothesis that during tribological testing, the initial W(VI) partially undergoes reduction reaction(s), producing the observed compounds and allowing the formation of the tribofilm. The presence of these reduced oxidation states deeper in the metal surface can be explained by the material smearing action during the test, which induces both physical and chemical changes in the material. This "physicochemical smearing" process had not yet affected the shallower surface,

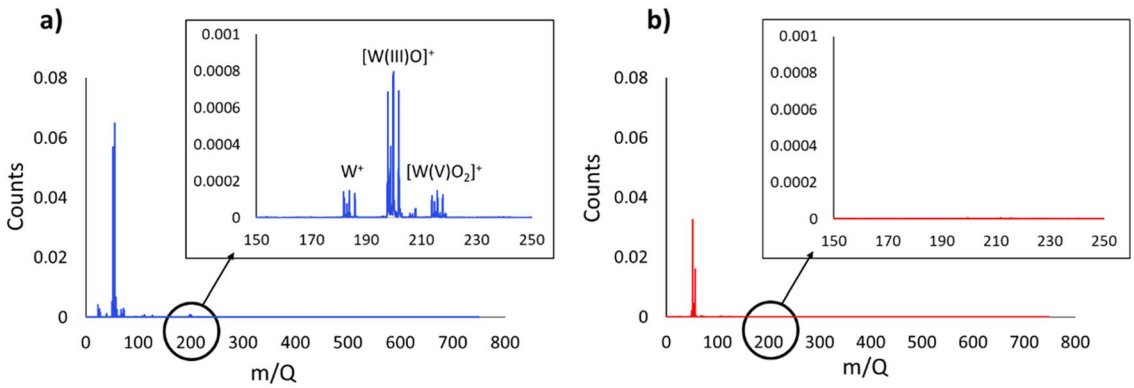

Fig. 7 ToF-SIMS analysis of (a) inside and (b) outside the wear track of SiW_{11}THTDA in PAO8.

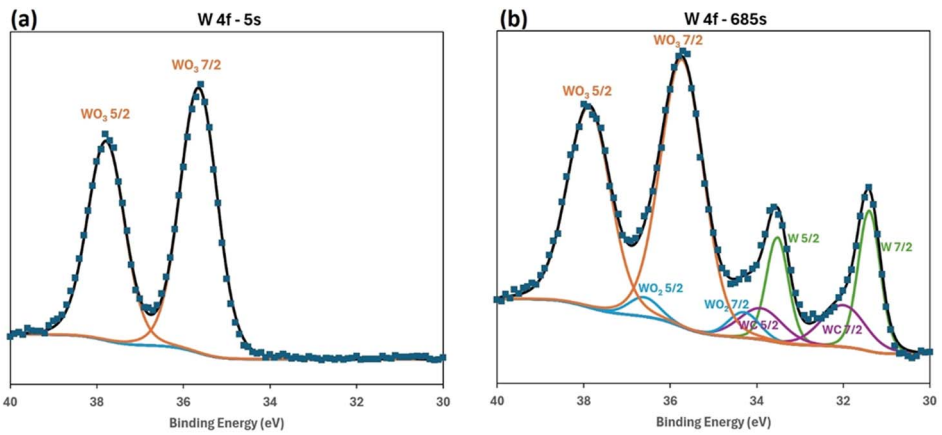

Fig. 8 XPS analysis inside the wear track of SiW_{11}THTDA in PAO8 showing the presence of tungsten at (a) 5 seconds and (b) 685 seconds etch time.

Table 5 Summary of friction, wear, adsorption, and tribofilm analysis for SiW_{11}THTDA and ZDDP in PAO8 and DPG

		Friction				
Base fluid	Additive	Running in (m)	Stabilized COF	Wear (mm^2 Nm^{-1})	Adsorption	Tribofilm
PAO8	POM-IL	~12.5	~0.12	$\sim 4.7 \times 10^{-6}$	Chemisorption	Full coverage, O-rich, presence of W
	ZDDP	~5.25	~0.12	$\sim 3.7 \times 10^{-6}$	Physisorption	Patchy, presence of O, S, P and Zn
DPG	POM-IL	~0	~0.16	$\sim 4.4 \times 10^{-5}$	Physisorption	Not observed
	ZDDP	~0.5	~0.16	$\sim 3.4 \times 10^{-5}$	Physisorption	Not observed

where changes in W oxidation state were less significant. Nevertheless, potential reducing effects of XPS etching should also be considered before drawing definite conclusions, particularly given the differing oxidation states detected by ToF-SIMS and XPS. This suggests a high likelihood of significant changes in oxidation states, but the analytical techniques used in this work do not provide conclusive insight into the exact oxidation states present.

As expected, the lubricant formulation containing ZDDP in PAO8 also formed a tribofilm on the metal surface, as can be seen in both the S(T)EM and EDS images (Fig. 3 and S7†). This tribofilm was patch-like in structure, with oxides, P, S, and Zn, likely in the form of polyphosphates and sulphides, as published in previous studies.[39,47] This confirms that a tribochemical reaction has occurred although the QCM study showed full desorption of ZDDP upon flushing with plain PAO8. This confirms that QCM alone is not enough to account for tribochemical reactions during a tribo-process. Previous literature indicates the ease of thermal decomposition of ZDDP, ranging from 130 to 230 °C, depending on its alkyl chain.[47,48] Therefore, the products of this decomposition and the high local temperatures of the tribo-process are expected to result in a tribochemical surface reaction even if the additive is only physisorbed. Whereas for the POM-IL, the chemisorption process aided the higher temperature needed for the additive to decompose and form a tribofilm.

For DPG, no evidence of functional additives was found, as shown by the lack of tribofilm formation in Fig. 4. The interaction between the base fluid and the additives resulted in a competition for the surface adsorption sites, likely due to the size of DPG as well as its polar and mildly aliphatic nature (Table 2), preventing the additives from efficiently reaching the surface. Consequently, no tribochemical reactions occur at the surface thus resulting in higher friction and wear.

4.3. The effect of tribofilm and adsorption on friction and wear

There is no singe method for forming a tribofilm, its composition can still vary while maintaining its protective properties. Table 5 provides an overview of the different adsorption and the tribofilm characteristics of each additive and how these translate to similar friction and wear results.

The inability of ZDDP and SiW_{11}THTDA to efficiently reach the metal surface in DPG likely applies to the other additives as well. Therefore, despite their good solubility, they do not improve friction and wear due to surface site competition with the base fluid (Fig. 1 and Table 4). Only ZDDP seemed to result in a minor decrease in wear compared with the other additives, likely because its lower decomposition temperature.

The esters appear to behave similarly to DPG, with a significant reduction in wear for DhL4018 with additives and significantly lower wear rate values for ZDDP in DhL4016, suggesting a tribochemical reaction likely occurred, leading to tribofilm formation. In polar base fluids like esters and glycols, the effect of the base fluid on the substrate leads to adsorption competition with the additives, ultimately overpowering their performance with respect to the additives. In addition, given the intrinsic nature of esters as friction-reducing agents in lubricants,[32] a further reduction in friction provided by additives would be difficult to observe.

The longer running-in period observed for all PAO8 formulations, along with the strong metal surface deformation and surface chemistry modification, suggests that the test begun with a stage of high energy and significant physicochemical changes in the system (metal surface and lubricant). Following the running-in period, a protective layer forms, reducing both friction and wear for both tested additives. The shorter running-in period for ZDDP suggests a faster tribochemical process than for SiW_{11}THTDA. This is supported by evidence of a faster thermal decomposition of ZDDP, which can occur at temperatures around 200 °C.[48] In contrast, POM-ILs start to decompose at higher temperatures, between 200 and 600 °C (Fig. S8†). The high decomposition temperature for POM-ILs suggest they might be more suitable as extreme pressure additives. Indeed, an indirect confirmation for that is the longer running-in period and the larger recrystallization area observed in the FIB cross section and the STEM image of SiW_{11}THTDA in PAO8 (Fig. 3). The higher decomposition temperature for the POM-IL requires a longer time to activate the tribochemical reactions on the surface but the strong adsorption of this additive to the metal surface (Fig. 5) aids that process making it possible to form a tribofilm under less demanding mechanochemical conditions indicating it can also act as an anti-wear additive reaching average values similar to ZDDP.

5. Conclusions

Polyoxometalate ionic liquids (POM-ILs) have been studied as potential lubricant additives in different base fluids. Overall, the POM-IL family showed promising results as lubricant

additives, with their tuneable properties offering significant potential for further study. It is the hope that this work will promote the interest in these structures within the tribology community. Based on the experimental data obtained in this work, the following conclusions can be drawn:

This family of compounds has a complex structure, making their compatibility behaviour difficult to predict. However, both emulsions and well-solubilized lubricants can be successfully prepared.

The wear and friction-reducing action of POM-ILs are significant and comparable to those of well-known additives, such as ZDDP. However, their performance is highly dependent on the base fluid used and their ability to efficiently interact with the tribo-surface.

Adsorption studies demonstrate that POM-ILs strongly adsorb onto a stainless steel coated sensor under static conditions. However, the choice of base fluid can significantly influence this ability, especially when competing adsorption processes are at play.

Advanced surface analysis using FIB, STEM, EDS, and ToF-SIMS revealed the formation of a mostly oxide-rich and also W-containing tribofilm, with homogeneous coverage, which appears to result from the decomposition of SiW_{11}THTDA and subsequent reaction with the stainless steel surface.

ToF-SIMS data, supported by XPS analysis, suggests a potential change in oxidation state of tungsten with depth. It was observed that reduction reaction(s) increased the prevalence of oxidation states different from the original in the POM-IL (VI) to IV and 0. This change in oxidation state may be due to the smearing process that physically and chemically modifies both the metal surface and the lubricant formulation. However, as XPS and ToF-SIMS can influence the sample itself, further studies are necessary to confirm these findings.

Data availability

The data supporting this article have been included as part of the ESI.† In addition, all data used for this article are included in the main figures of the manuscript.

Conflicts of interest

There are no conflicts to declare.

Acknowledgements

The authors would like to acknowledge financial support from the Norwegian Infrastructure for Micro- and Nanofabrication (NORFAB, project 295864), the Infrastructure for Materials Research for Transporting Hydrogen (SMART-H, project 296197) and the enabling technologies at NTNU (project 81771596). This work was funded through the grant PID2022-141276OB-I00 and CEX2023-001286-S funded by MCIN/AEI/10.13039/501100011033 (Ministerio de Ciencia e Innovación/Agencia Estatal de Investigación, Spain). This study was supported by MCIN with funding from the European Union NextGenerationEU (PRTR-C17.I1) promoted by the Government of Aragón. The authors acknowledge the Laboratorio de Microscopias Avanzadas (LMA) at the University of Zaragoza for offering access to their instruments and expertise. M.-L. C. acknowledges COST Action CA20130 "Euro-MIC" for an STSM grant.

References

1 K. Holmberg and A. Erdemir, *Tribol. Int.*, 2019, **135**, 389–396.
2 K. Holmberg and A. Erdemir, *Friction*, 2017, **5**, 263–284.
3 K. Holmberg, P. Andersson and A. Erdemir, *Tribol. Int.*, 2012, **47**, 221–234.
4 P. Nowak, K. Kucharska and M. Kami, *Int. J. Environ. Res. Public Health*, 2019, **16**, 1–13.
5 K. Skyberg, V. Skaug, B. Gylseth, J. R. Pedersen and O. H. Iversen, *Environ. Res.*, 1990, **53**, 48–61.
6 *Lubricant Additives: Chemistry and Applications*, L. R. Rudnick, ed, CRC Press, 2nd edn, 2009.
7 M. Cai, Q. Yu, W. Liu and F. Zhou, *Chem. Soc. Rev.*, 2020, **49**, 7753–7818.
8 C. D. Hubbard, P. Illner and R. Van Eldik, *Chem. Soc. Rev.*, 2011, **40**, 272–290.
9 H. Khanmohammadi, W. Wijanarko and N. Espallargas, *Tribol. Lett.*, 2020, **68**, 1–15.
10 Y. Chen, P. Renner and H. Liang, *Friction*, 2023, **11**, 489–512.
11 D. Wei, R. Dong, H. Xu, X. Wang, X. Liu and Y. Liang, *Tribol. Int.*, 2023, **184**, 108430.
12 H. Xiao, *Tribol. Trans.*, 2017, **60**, 20–30.
13 S. Kawada, S. Watanabe, Y. Kondo, R. Tsuboi and S. Sasaki, *Tribol. Lett.*, 2014, **54**, 309–315.
14 W. Wijanarko, H. Khanmohammadi and N. Espallargas, *Langmuir*, 2022, **38**(9), 2777–2792.
15 Y. Zhou and J. Qu, *ACS Appl. Mater. Interfaces*, 2017, **9**, 3209–3222.
16 A. Romero, A. Santos, J. Tojo and A. Rodr, *J. Hazard. Mater.*, 2008, **151**, 268–273.
17 R. P. Swatloski, J. D. Holbrey and R. D. Rogers, *Green Chem.*, 2003, 361–363.
18 P. Rohlmann, J. J. Black, S. Watanabe, J. Leckner, M. R. Shimpi, M. W. Rutland, J. B. Harper and S. Glavatskih, *Tribol. Int.*, 2023, **181**, 108263.
19 S. Zhang, L. Ma, P. Wen, X. Ye, R. Dong, W. Sun, M. Fan, D. Yang, F. Zhou and W. Liu, *Tribol. Int.*, 2018, **121**, 435–441.
20 C. Jiang, W. Li, J. Nian, W. Lou and X. Wang, *Friction*, 2018, **6**, 208–218.
21 J. J. Berzelius, *Ann. Phys.*, 1826, **82**, 331–350.
22 Y. Zhou, G. Chen, Z. Long and J. Wang, *RSC Adv.*, 2014, **4**, 42092–42113.
23 A. Misra, I. Franco Castillo, D. P. Müller, C. González, S. Eyssautier-Chuine, A. Ziegler, J. M. de la Fuente, S. G. Mitchell and C. Streb, *Angew. Chem., Int. Ed.*, 2018, **57**, 14926–14931.
24 H. Soria Carrera, E. Atrian Blasco, J. Martinez de la Fuente, S. G. Mitchell and R. Martín-Rapún, *Nanoscale*, 2022, **14**, 5999.
25 F. Boussema, R. Haddad, Y. Ghandour, M. S. Belkhiria, M. Holzinger, A. Maaref and S. Cosnier, *Electrochim. Acta*, 2016, **222**, 402–408.

26 S. Herrmann, L. De Matteis, J. M. de la Fuente, S. G. Mitchell and C. Streb, *Angew. Chem., Int. Ed.*, 2017, **56**, 1667–1670.
27 Y. Martinetto, S. Basset, B. Pégot, C. Roch-Marchal, F. Camerel, J. Jeftic, B. Cottyn-Boitte, E. Magnier and S. Floquet, *Molecules*, 2021, **26**, 1–18.
28 K. Rajkowska, A. Koziróg, A. Otlewska, M. Piotrowska, E. Atrián-Blasco, I. Franco-Castillo and S. G. Mitchell, *Molecules*, 2020, **25**(23), 5663.
29 M. J. da Silva, P. H. da Silva Andrade, S. O. Ferreira, C. B. Vilanculo and C. M. Oliveira, *Catal. Lett.*, 2018, **148**, 2516–2527.
30 L. Matczak, C. Johanning, E. Gil, H. Guo, T. W. Smith, M. Schertzer and P. Iglesias, *Tribol. Int.*, 2018, **124**, 23–33.
31 L. Taylor, A. Dratva and H. A. Spikes, *Tribol. Trans.*, 2000, **43**, 469–479.
32 L. R. Rudnick, *Synthetics, Mineral Oils, and Bio-Based Lubricants*, CRC Press, Boca Raton, Florida (USA), 2nd edn, 2020.
33 L. Bjerregaard, K. Geels, B. Ottesen and M. Rückert, Metalog guide. Your Guide to the Perfect Materialographic Structure, *Struers A/S*, Rødovre (Denmark), 2020.
34 D. D. Bernard and J. Hamrock, *Ball Bearing Lubrication : The Elastohydrodynamics of Elliptical Contacts*, Wiley, 1981.
35 R. W. Bruce, *Handbook of Lubrication and Tribology. Volume II: Thory and Design*, CRC Press, Boca Raton, Florida (USA), 2012.
36 J. F. Archard, *J. Appl. Phys.*, 1953, 981–988.
37 N. I. Gumerova and A. Rompel, *Chem. Soc. Rev.*, 2020, **49**, 7568.
38 H. Dang, L. Sun, J. Zhou and Z. Zhang, *Tribol. Lett.*, 2004, **17**, 311–316.
39 C. Minfray, J. M. Martin, M. I. De Barros, T. Le Mogne, R. Kersting and B. Hagenhoff, *Tribol. Lett.*, 2004, **17**, 351–357.
40 G. Sauerbrey, *Physik*, 1959, **155**, 206–222.
41 M. V. Fedorov and A. A. Kornyshev, *Chem. Rev.*, 2014, **114**, 2978–3036.
42 C. S. Perez-Martinez and S. Perkin, *Langmuir*, 2019, **35**, 15444–15450.
43 A. G. Enderle, I. Franco-Castillo, E. Atrián-Blasco, R. Martín-Rapún, L. Lizarraga, M. J. Culzoni, M. Bollini, J. M. De La Fuente, F. Silva, C. Streb and S. G. Mitchell, *ACS Appl. Polym. Mater.*, 2022, **4**(6), 4144–4153.
44 C. Bittencourt, M. P. Felicissimo, A. Felten, L. A. O. Nunes, P. Ivanov, E. Llobet, J. J. Pireaux and L. Houssiau, *Appl. Surf. Sci.*, 2005, **250**, 21–28.
45 J. Jurczyk, L. Pillatsch, L. Berger, A. Priebe, K. Madajska, C. Kapusta, I. B. Szymanska, J. Michler and I. Utke, *Nanomaterials*, 2022, **12**, 2710.
46 W. Wijanarko, H. Khanmohammadi and N. Espallargas, *Friction*, 2022, **10**, 1405–1423.
47 H. Spikes, *Tribol. Lett.*, 2004, **17**, 469–489.
48 M. Z. Huq, X. Chen, P. B. Aswath and R. L. Elsenbaumer, *Tribol. Lett.*, 2005, **19**, 127–134.